The Total Electron Content from InSAR and GNSS: a mid-latitude study.

Elvira Musicò, Claudio Cesaroni, Luca Spogli, John Peter Merryman Boncori, Giorgiana De Franceschi, Roberto Seu

1

***Abstract* – The Total Electron Content (TEC) measured from InSAR (Interferometric Synthetic Aperture Radar) and from a dense network of GNSS (Global Navigation Satellite System) receivers is used to assess the capability of InSAR to retrieve ionospheric information when the tropospheric contribution to the interferometric phase is reasonably negligible. With this aim, we select three night time case studies over Italy and investigate the correlation between TEC from ALOS (Advanced Land Observing Satellite)-PALSAR (Phased Array type L-band Synthetic Aperture Radar) and from the RING (Rete Integrata Nazionale GPS) network, the latter considered as the reference true ionospheric TEC. To retrieve the TEC variability from ALOS-PALSAR, we firstly investigate the correlation between the integral of the azimuth shifts and the interferometric phase in the absence of ground motions (e.g. earthquakes) and/or heavy rain events. If correlation exists (as in two out of three case studies under investigation) we can assume the tropospheric contribution to the interferometric phase as negligible and the TEC variability from L-band InSAR can be retrieved. For these two case studies, the comparison between the TEC from the InSAR images and from the RING network is quite encouraging as the correlation coefficient is R~0.67 in the first case and R~0.83 in the second case. This result highlights the potential to combine InSAR and GNSS experimental measurements to investigate small-scale spatial variability of TEC, in particular over regions scarcely covered by ground-based GNSS receivers.**

IEEE keywords — Ionosphere, Synthetic Aperture Radar, Global Positioning System

I. INTRODUCTION

THE Interferometric Synthetic Aperture RADAR (InSAR) is one of the most used techniques for geophysical applications, as it provides, among the others, maps of surface deformation with high accuracy (mm level). The signals emitted by low frequency space-borne SAR (Synthetic Aperture Radar) are affected by the presence of the neutral and ionized atmosphere (troposphere and ionosphere). This leads to an additional phase contribution to the interferogram and, consequently, to an error in, e.g., the displacement measurement [1]. This additional phase is the sum of two different terms: the tropospheric phase delay and the ionospheric phase advance. The ionospheric phase advance [2] [3] depends on the temporal ionospheric variability between different passages of SAR over the selected region. In addition, the spatial ionospheric variability may cause "phase gradients" across the azimuth chirp [4]. These phase gradients are responsible for the so-called "azimuth streaking" pattern in the optimal azimuth co-registration shifts of InSAR pairs [5] [6]. Such ionospheric features can be expressed in terms of the ionospheric Total Electron Content (TEC). Despite the ionospheric phase advance poses a threat on InSAR signals, this may be conversely used to retrieve the TEC variability in both space and time. However, independent experimental observations of the ionospheric plasma would be necessary to assess the reliability of such TEC-from-SAR data derivation.

In the recent literature, the ionospheric issues on SAR have been faced mainly by using

representations of the ionospheric conditions at a global level. This may be inaccurate for InSAR applications. In the specific, global TEC maps, such as the GIM's (Global Ionosphere Map, http://iono.jpl.nasa.gov/gim.html), suffer by low spatial resolution, as they are typically available on regular grids 2.5° latitude times 5° longitude. On the other hand, approaches based upon global models, such as the WBMOD (WideBand MODel, https://spawx.nwra.com/ionoscint/wbmod.html) [7], provide only average ionospheric conditions that may be insufficient to detail local transient ionospheric phenomena.

Suitable ionospheric information to address InSAR can be obtained from regional dense networks of GNSS receivers. Here we investigate, for three case studies at mid-latitude during nighttime, the possibility to retrieve TEC from InSAR by using as the "true reference ionosphere" the TEC measured by a local dense network of GPS receivers. Such a network ensures an accuracy on the TEC variability estimation that can be compared with that one obtained with InSAR. This can be done by assuming, under some conditions, the tropospheric contribution to the interferometric phase as negligible with respect to the ionospheric contribution. In the specific, we present the results obtained by comparing TEC variations derived from: i) ALOS-PALSAR master and slave images over central Italy, and ii) the RING (Rete Integrata Nazionale GPS, http://ring.gm.ingv.it//) network, managed by the Istituto Nazionale di Geofisica e Vulcanologia (Italy).

In Section II, we describe the analysis method to retrieve the TEC temporal variation (ΔTEC) from the interferometric phase once the condition of negligible troposphere in respect to the ionosphere is satisfied. Then, details are given on the ΔTEC evaluation from RING, based on the hypothesis of a "frozen" ionosphere within a time interval of 5 minutes around the corresponding ALOS passages, and adopted to count for the ionospheric mapping needs. In Section III, the comparisons between the two independent ΔTECs (from InSAR and from GNSS) are shown and discussed for the case studies under investigation. Then, in Section IV, conclusions are given and the next steps of the investigation are suggested.

II. ANALYSIS METHOD

In these case studies, we use *i)* images acquired over central Italy by ALOS-PALSAR and *ii)* TEC from RINEX (Receiver INdependent EXchange format) data provided by the RING network, for three epochs: 1 July 2007, 16 August 2007 and 1 October 2007, around 21.29 UT.

A. Δ*TEC from InSAR*

An interferogram is generated by cross-correlating two SAR images, a "master" and a "slave", acquired over the same area [1]. For a SAR operating in repeat-pass mode, the interferometric phase is given by the phase difference between two SAR coregistrated images. If no meaningful movements of the ground occur in the period between the two passages (e.g., earthquakes), using a Digital Elevation Model (DEM) and after the removal of the shift due to parallel baseline by using precise orbits [1], the interferometric phase is due mainly to the atmospheric (ionospheric and tropospheric). Then, the interferometric phase can be expressed as follows:

$$\Delta\varphi = \Delta\varphi_{atm} = \Delta\varphi_{tropo} + \Delta\varphi_{iono}\,; \qquad (1)$$

where $\Delta\varphi_{iono}$, according to [8], is :

$$\Delta\varphi_{iono} = \frac{4\pi}{c}\frac{K}{f}\,\Delta TEC; \qquad (2)$$

in which f is the central frequency (in Hz), c is the speed of light, K=40.3 m^3/s^2 is a constant and ΔTEC is the TEC difference between two passages:

$$\Delta TEC = TEC_m - TEC_s. \qquad (3)$$

In (3), TEC_m and TEC_s are the TEC values at the acquisition time of the master and slave images, respectively. TEC is expressed in TEC units [TECu]: 1 TECu = 10^{16} electrons·m^{-2}.

To retrieve ΔTEC from the interferometric phase $\Delta\varphi$, we must assume $\Delta\varphi_{tropo}$ as negligible with respect to $\Delta\varphi_{iono}$ in *(1)*. To identify when such condition is satisfied, we apply a method based on the correlation between the integral of the azimuth shifts (Δx) and the interferometric phase ($\Delta\varphi$). The main steps of such method are detailed below.

As introduced by [3] and further investigated by [4], the azimuth shift Δx is proportional to the gradient of the ionospheric phase along the azimuth direction

($\frac{\partial \Delta\varphi_{\text{iono}}}{\partial \text{x}}$), then, taking into account *(2)*, Δx results to be proportional to the gradient of ΔTEC along the azimuth direction [9]:

$$\Delta x \propto \frac{\partial \Delta TEC}{\partial x}. \quad (4)$$

Therefore, the integral in *(4)* is proportional to ΔTEC:

$$\int \Delta x \, dx \propto \Delta TEC \quad (5)$$

The integral in *(5)*, a part an unknown integration constant, can be calculated by using a cumulative numerical integration. Starting from an M × N array of shifts, where M and N are the number of pixels in azimuth and range respectively, the integral is given by:

$$\begin{cases} \Delta x(1,j) \approx \Delta\varphi_{iono}(1,j) \propto \Delta TEC(1,j) \quad if\ i = 1 \\ \Delta x(i,j) + \sum_{n=2}^{i} [\,\Delta x(n-1,j)] \approx \Delta\varphi_{iono}(i,j) \\ \qquad \propto \Delta TEC(i,j) \ \ if\ i > 1 \end{cases}$$

$$\forall\, i = 1 \ldots . M \ and \ j = 1 \ldots N \quad (6)$$

where $\Delta\varphi_{iono}(i,j)$ is the contribution of the ionosphere to the interferometric phase in the pixel *(i,j)* and the terms $\Delta TEC(i,j)$ are the differences between TEC at master and slave passages in the pixel *(i,j)*.

If correlation exists between the integral of azimuth shifts $\int \Delta \text{x}\, \text{dx}$ from *(6)* and the (unwrapped) interferometric phase $\Delta\varphi$ from (1), then we can assume $\Delta\varphi_{tropo}$ negligible. This follows from *(5)*, where the integral of the azimuth shifts is only proportional to ΔTEC. The azimuth shifts Δx are estimated by using the Multiple Aperture InSAR (MAI) method ([10] and [11]).

We apply this analysis method to the SAR images acquired in "repeat-pass interferometry mode" during three different epochs (1 July 2007, 16 August 2007 and 1 October 2007, around 21.29 UT). The characteristics of the SAR images acquisition mode are reported in Table 1.

B. ΔTEC *from RING*

TEC is the measure of the total amount of free electrons/ions present along the transmitter-to-receiver path, which, in the case of GNSS measurements, crosses the whole ionosphere. TEC depends on local time, season, geographic coordinates, geospace and thermosphere conditions, therefore it is a highly variable quantity.

The concentration of free electrons/ions significantly affects the propagation of the GNSS signals through the ionosphere. In particular, it causes a transmission delay proportional to the slant TEC (*sTEC*), defined as the TEC along each slant path:

$$sTEC = \int_L n_e(l)\, dl\ . \quad (7)$$

In *(7)*, n_e is the electron density and L is the ray path of the satellite-receiver link.

Starting from code and carrier phase data acquired by dual-frequency GNSS receivers located at ground, it is possible to calculate *sTEC* (in TECu), according to the following formula:

$$sTEC = \frac{1}{K}\left(\frac{L1^2 L2^2}{L2^2 - L1^2}\right)(P_2 - P_1) - \varepsilon, \quad (8)$$

where *L1* (1575.42 MHz) and *L2* (1227.60 MHz) are the two frequencies of the transmitted signal, $P1$ and $P2$ are the corresponding pseudoranges and ε represents all the biases induced by the receiver, satellite, multipath etc.

The minimization of the biases is a very delicate issue of the TEC determination from GNSS: it is necessary to apply a calibration procedure [12] to obtain reliable TEC values. In this work, the GOPI software (http://seemala.blogspot.it/2011/04/rinex-gps-tec-program-version-22.html) has been used for the TEC calibration. This software provides, for each satellite-receiver link, *sTEC* values projected to the vertical (hereafter TEC_{GNSS}), assuming that the ionosphere is a thin, ionized layer located at 350 km above the Earth's surface [13]. This assumption is commonly adopted and it is quite reasonable for the mid-latitude ionosphere. An advantage of this projection is the provision of TEC values independent on the geometry of the GNSS constellation and of the receiver's network.

As stated in Section I, a very dense network of GNSS receivers allows the ionosphere mapping (in terms of TEC_{GNSS}) with high spatial resolution. To the scope, we use data acquired by RING, constituted by about 180 receivers covering the Italian territory (Fig. 1).

As the investigation refers to mid-latitude, nighttime case studies, we assume the ionosphere as "frozen" (i.e. not meaningfully changing) during a time interval of 5 minutes around each passage of ALOS. This assumption allows increasing the number of IPP's (Ionospheric Pierce Point, assumed at 350 km) simultaneously available within the time interval in which the ionosphere can be considered stable. This improves the spatial coverage and, consequently, the interpolation performance (as described below). To obtain TEC_{GNSS} maps, representing the TEC distribution during the time of ALOS passage, we consider TEC values (30 sec sampling rate) at all IPP's (between 30°-60°N and 5°-20° E) during the above mentioned 5-minutes interval. These values at the IPP's are then interpolated with the natural neighbour method [14]. Such method is quite effective in depicting strong TEC variability as occurring, e.g., at equatorial regions [15]. Thus, maps of interpolated TEC_{GNSS} are obtained over a regular grid of 0.01° in latitude x 0.01° in longitude. From these maps, we select only the portion of the

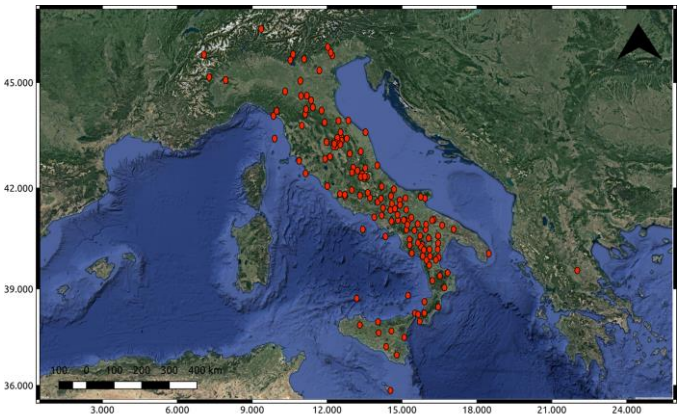

Fig. 1. RING (Rete Integrata Nazionale GPS) network http://ring.gm.ingv.it/.

ionosphere crossed by the ALOS-PALSAR signals during the image acquisition. Interpolating before the selection of the area of interest (sub map) keeps the mapping safe from border effects induced by the interpolation itself.

The ionospheric portion crossed by the ALOS-PALSAR signals is a delicate issue of the technique and it is here estimated by:

- calculating the SAR position vector in ECR (Earth-Centered Rotational) coordinates;
- computing, pixel by pixel, the SAR line-of-sight and its intersection with a thin-shell ionosphere at a constant height of 350 km above the ellipsoid of reference (WGS84, Fig 2b).

The resulting portion of the ionosphere crossed by ALOS-PALSAR signals (within the black rectangle) and the corresponding image area at ground (within the red rectangle) are plotted in Fig. 2a.

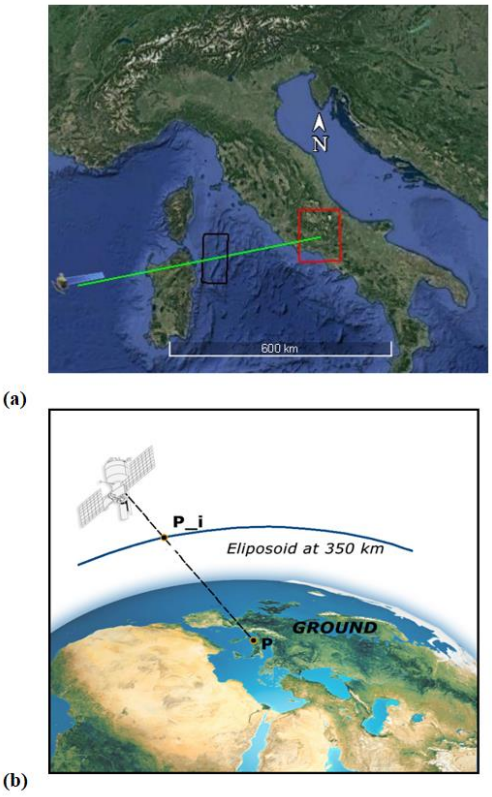

Fig. 2. Ionosphere crossed by SAR signal. Panel (a) shows the portion of the ionosphere (black rectangle) at 350 Km crossed by ALOS-PALSAR signals and the corresponding image area at ground (red rectangle). Panel (b) sketches how to found the IPP: P is the point at ground and P_i is the intersection between the SAR signal and the ellipsoid projected at 350 km (altitude of the thin ionospheric shell).

Being located at 350 km, the TEC_{GNSS} sub map size is smaller than that one of the InSAR image at ground. The necessary resizing is obtained by projecting each couple of coordinates of the TEC_{GNSS} grid on the georeferenced InSAR image. Moreover, the ΔTEC_{SAR} map resolution ($8.33°\cdot10^{-4}$ latitude x $8.33°\cdot10^{-4}$ longitude) is higher than that one of the TEC_{GNSS} sub map (0.01° latitude x 0.01° longitude). To overcome this issue, we resample the TEC_{GNSS} sub map (up to $8.33°\cdot10^{-4}$) by applying a linear interpolation on TEC_{GNSS} values both in latitude and in longitude.

Finally, to account for the TEC_{GNSS} spatial and temporal variation (pixel by pixel) between two

ALOS passages, we calculate the map of ΔTEC_{GNSS} grid values according to the following formula:

$$\Delta TEC_{GNSS} = (TEC_{GNSS_m} - TEC_{GNSS_s}); \quad (9)$$

in which TEC_{GNSSm} and TEC_{GNSSs} are the TEC_{GNSS} grid map values relative to 5 minutes around the master (*m*) and slave (*s*) passages of ALOS, respectively. In order to compare ΔTEC_{SAR} and ΔTEC_{GNSS} maps, we subtracted to each value $\Delta TEC_{GNSS}(Lat_i,Lon_i)$, where (Lat_i,Lon_i) are the coordinates of the generic grid point, the value $\Delta TEC_{GNSS}(Lat_0,Lon_0)$. The coordinates (Lat_0,Lon_0) are the same of the point that we used as the reference to unwrap the interferometric phase.
In the following section, the results of the proposed analysis are shown for the case studies under investigation.

III. Results and Discussion

As stated in Section II, we evaluate and compare ΔTEC_{SAR} and ΔTEC_{GNSS} from the interferometric images and from the RING network, respectively. Three images, acquired by ALOS-PALSAR (ground track 638) over central Italy around 21:29 UT in three different epochs are selected. Dates and the relative acquisition characteristics are reported in Table 1.

TABLE 1
Date of the master/slave images and their acquisition characteristics. Θ_M and Θ_S are the incidence angle of the master and the slave image, respectively. B_T stands for the temporal baseline and B_P stands for perpendicular baseline.

Case study	**#1**	**#2**	**#3**
Master	**1 July 2007**	**16 August 2007**	**1 July 2007**
Slave	**16 August 2007**	**1 October 2007**	**1 October 2007**
θm (°)	38.7191	38.7395	38.7191
θs (°)	38.7395	38.7223	38.7223
Bt (days)	46	46	92
Bp (m)	279.9401	259.2523	539.2134
Chirp Bandwith	14 MHz	14 MHz	14 MHz

Three images at the epochs: 1 July, 16 August, and 1 October 2017 are suitable combined to determine the three case studies under investigation:

- case #1 and #3 share the same master image;
- case #2 and #3 share the same slave image;
- case #2 master image is the slave image of case #1.

The knowledge of the geomagnetic conditions at a given epoch is useful to reveal, if any, the ionosphere main features that may occur under disturbed geospace conditions [16]. The ALOS-PALSAR passages on 1 July, 16 August and 1 October 2007, were characterized by quiet geomagnetic conditions, as highlighted by the Dst, AU/AL/AE and Kp geomagnetic indices, available at the website of the Kyoto World Data Center (wdc.kugi.kyoto-u.ac.jp). In addition, for each case studies, to look for the dynamics of local ionospheric disturbances around the images acquisition times, we consider the experimental observations (ionograms) from the DPS-4 ionosonde (HF radar) at the INGV Rome observatory (41.8° N, 12.5° E), performed from 21:00 UT to 21:45 UT. An ionogram provides the trend of the virtual height of the ionospheric layers as function of the transmitted signal frequency [17].
Fig. 3 shows the ionograms on 1 July 2007. The critical frequency of the F2 layer (*foF2* [18]) ranges from 5.5 to 6 MHz at a virtual height (*h'F*) of about 250 km. A weak sporadic-E layer (*Es*), with a critical frequency, *foEs*, of about 3 MHz, occurs during the image acquisition, at a virtual height of about 100 km. The Es layer is a thin dense ionized plasma layer that sporadically appears in the lower part of the ionosphere, between 100 and 125 km. At mid latitude, the Es mainly occurs during summer [19], but its formation mechanisms is not fully assessed and understood, even if it seems linked to the presence of Atmospheric Gravity Waves (AGWs) [20] and to the Traveling Ionospheric Disturbances (TID's), i.e. the AGW manifestation in the ionosphere [21]. Day 16 August 2007 (Fig. 4) is characterized by a *foF2* of about 4.5 MHz, and a virtual height ranging from 212 km to 280 km. During the image acquisition, an Es occurs with *foEs* of about 5 MHz and *h'Es* of about 100 km.
The ionograms referring to 1 October 2007, shown in Fig. 5, are characterized by the sole presence of the expected night-time ionospheric F-layer. These ionograms, typical of the mid-latitude, autumn season, nighttime ionosphere, show a *h'F* ranging between 235 and 268 km and a *foF2* between 2.7 MHz and 2.9 MHz.

The occurrence of the Es layer on 16 August 2007 may affect SAR images ([22]). In fact, even if the associated Es frequency is low (*foEs*~5 MHz), this sporadic layer seems to be responsible for the streaks affecting the azimuth shifts maps referred to the case studies # 1 and #2, as reported below.

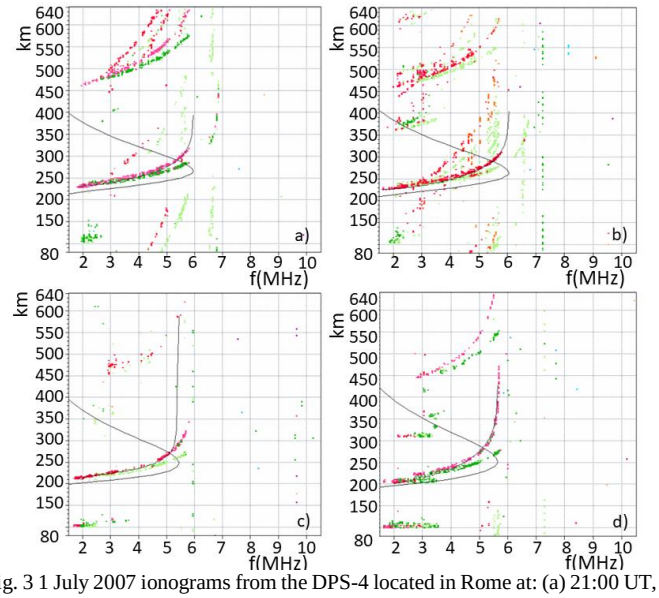

Fig. 3 1 July 2007 ionograms from the DPS-4 located in Rome at: (a) 21:00 UT, (b) 21:15 UT, (c) 21:30 UT, (d) 21:45 UT. The time of ALOS passage is around 21:29 UT. The black line is the modelled vertical electron density profile.

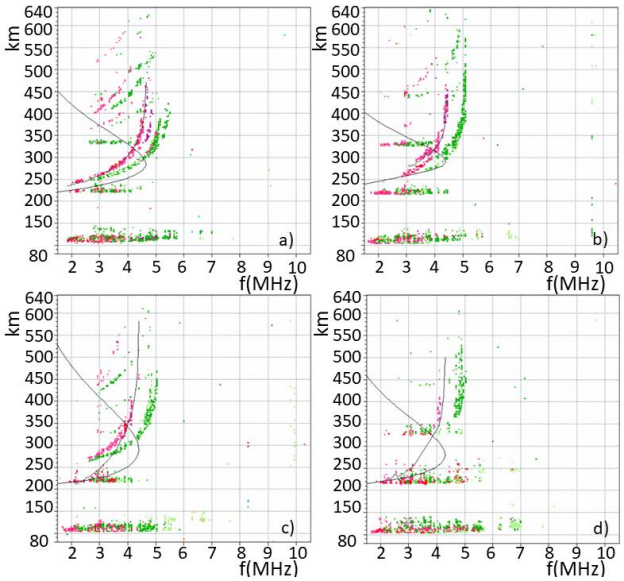

Fig. 4 16 August 2007 ionograms from the DPS-4 located in Rome at: (a) 21:00 UT, (b) 21:15 UT, (c) 21:30 UT, (d) 21:45 UT. The time of ALOS passage is around 21:29 UT. The black line is the modelled vertical electron density profile.

For each case study reported in Table 1, we evaluate:

- the azimuth shifts, Δx, from the MAI technique set with the parameters reported in Table 2;

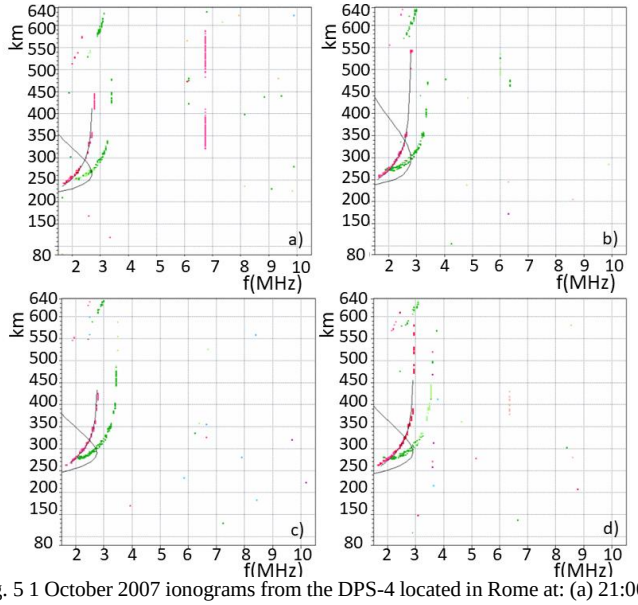

Fig. 5 1 October 2007 ionograms from the DPS-4 located in Rome at: (a) 21:00 UT, (b) 21:15 UT, (c) 21:30 UT, (d) 21:45 UT. The time of ALOS passage is around 21:29 UT. The black line is the modelled vertical electron density profile.

TABLE 2
PARAMETERS USED FOR MAI TECHNIQUE.

Parameter		Value
	normalized squint parameter	0.5
	azimuth multilook	20
	range multilook	8
Goldstein filtering	exponent for non-linear fitting	0.8
	filtering FFT window size	64
	coherence parameter estimation window size	7
	range step	4
	azimuth step	4
	minimum fraction of points required to be non-zero in the filter	0.9

- the integral of the azimuth shifts, $\int \Delta x$;
- the unwrapped phase, $\Delta\varphi$, unless the term associated to the unknown integer phase cycle ambiguity, $2\pi n$, [8];
- the correlation coefficient between $\int \Delta x$ and $\Delta\varphi$ to investigate if, for the selected case study, the tropospheric effect can be assumed negligible with respect to the ionospheric one.

The georeferenced maps of Δx, (Fig. 6, Fig. 7 and Fig. 8, panel a) show that the shifts vary from about -1 m to 1 m, in all the three case studies. We note similar patterns (but with opposite sign) for the first two case studies (Fig. 6 and Fig. 7, panel a) as they share 16 August 2007 as slave/master image in Fig. 6/Fig.7 (case study #1 and # 2, respectively). As

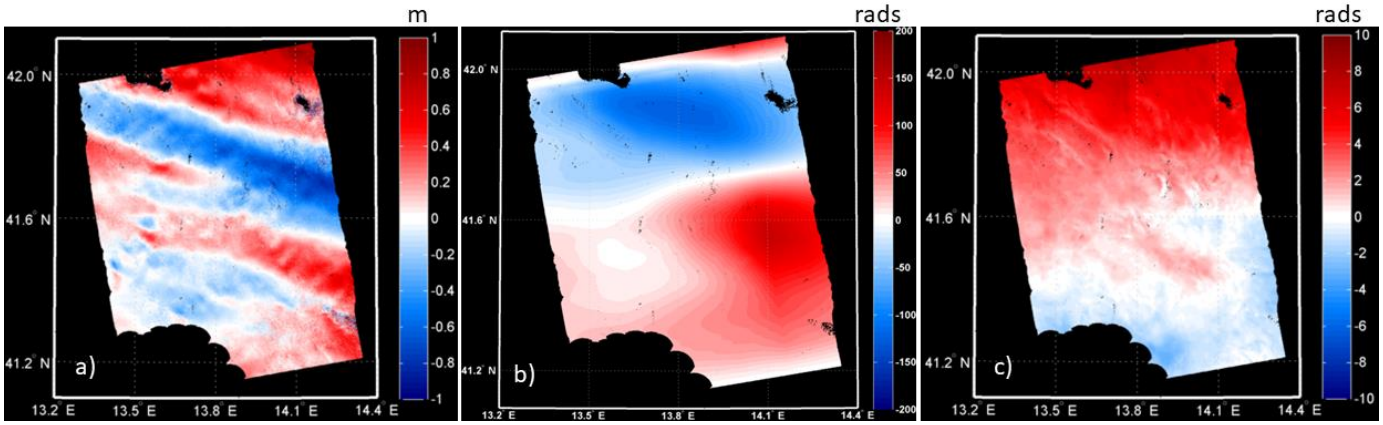

Fig. 6 Azimuth shifts (a), integral of the azimuth shifts (b) and unwrapped phase (c) refereed to the case study #1 (Table 1, 1 July 2007 and 16 August 2007 images used as master and slave, respectively). Colorbar for the panel (a) expresses the displacement in meters. To compare panel (b) with panel (c), both the integral of the azimuth shifts and the unwrapped phase are expressed in radians.

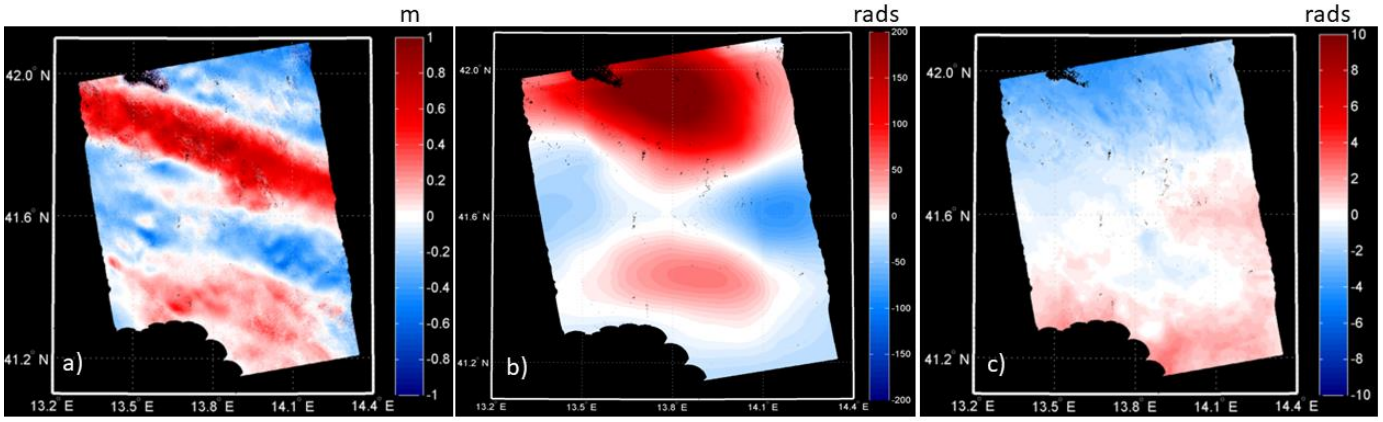

Fig. 7 Azimuth shifts (a), integral of the azimuth shifts (b) and unwrapped phase (c) refereed to the case study #2 (Table 1, 16 August 2007 and 1 October 2007 images used as master and slave, respectively). Colorbar for the panel (a) expresses the displacement in meters. To compare panel (b) with panel (c), both the integral of the azimuth shifts and the unwrapped phase are expressed in radians.

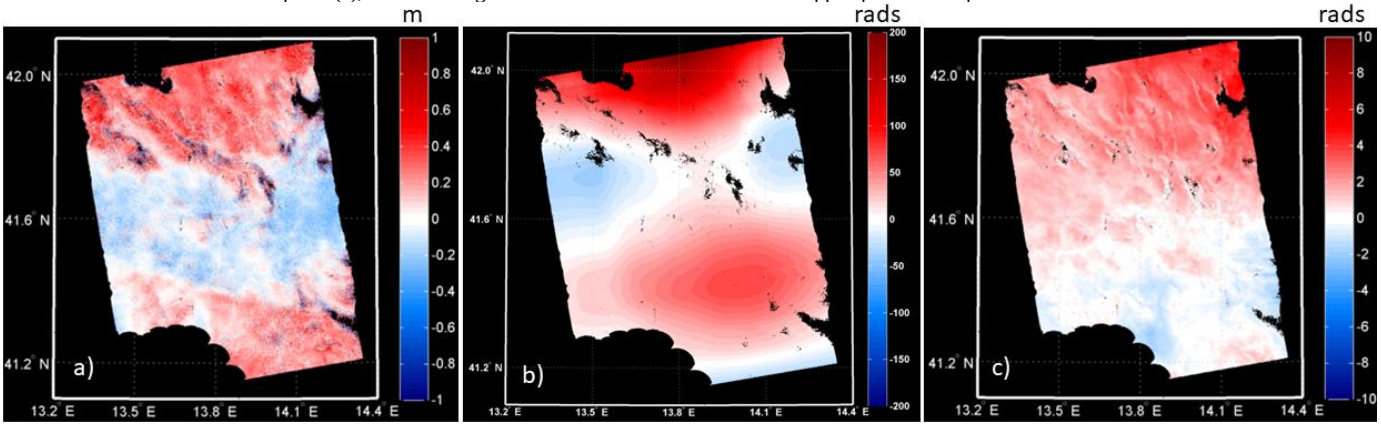

Fig. 8. Azimuth shifts (a), integral of the azimuth shifts (b) and unwrapped phase (c) refereed to the case study # 3 (Table 1, 1 July 2007 and 1 October 2007 images used as master and slave, respectively). Colorbar for the panel (a) expresses the displacement in meters. To compare panel (b) with panel (c), both the integral of the azimuth shifts and the unwrapped phase are expressed in radians.

mentioned above, we observe the presence of a marked azimuth streaking from about 41.6°N to 42°N. The streaking is absent in the case study #3 (Fig. 8 panel a). Since we use the SAR image of 16 August 2007 for both the case studies #1 and #2 but not for #3, we can argue that the occurrence of the Es layer with *foEs* threshold of, at least, 5 MHz (Fig. 4, panel c) may be the principal responsible for the streaks appearance.

Maps of the integral of the azimuth shifts, $\int \Delta x$, and of the unwrapped interferometric phase, $\Delta\varphi$, are shown in Fig. 6, Fig. 7 and Fig. 8, panels b and c. In order to account for the unknown integration constant, we add the range offsets (line by line) obtained by considering the differences (in range) between the integral of the azimuth shifts and the unwrapped interferometric phase.

In the case study #1 and #2 (Fig. 6 and Fig. 7), the correlation coefficients between the map of $\int \Delta x$ and

the map of $\Delta\varphi$ are R~-0.71 and R~-0.78, respectively. Such values of the correlation coefficients allow to consider negligible tropospheric effect condition as satisfied in (1) and to consequently retrieve ΔTEC_{SAR} by applying (2). The deviation from the ideal case ($|R|=1$) suggests that: i) the impact to the interferometric phase is not fully of ionospheric origin, and ii) the integration numerical error of (5) is not negligible.

In the case study #3 (Fig 8, panel b and c), the correlation coefficient is found to be R~0.2, which means that the tropospheric effect on the unwrapped interferometric phase cannot be neglected. In this case, we cannot extract ΔTEC_{SAR} from the interferogram.

Following what stated above, only for the case studies # 1 and #2 (Table 1), we can compare ΔTEC_{SAR} and ΔTEC_{GNSS}. Fig.9 shows maps of ΔTEC_{SAR} (panel a) and of ΔTEC_{GNSS} (panel b) for the case study #1. Similarly, Fig. 10 shows maps of ΔTEC_{SAR} (panel a) and of ΔTEC_{GNSS} (panel b) for the case study #2. These maps, provided by two independent experimental observations, are quite well correlated (R~0.67 for the case study #1 and R~0.83 for the case study #2). The corresponding scatter plots are shown in Fig. 11, panel a and b.

To check for the correctness of the assumptions upon which the method is based, we evaluated the correlation between ΔTEC_{SAR} and ΔTEC_{GNSS} also in case study #3, in which the assumption of negligible tropospheric effect is not satisfied. As expected, the correlation between the two independent ΔTEC measures is quite low (R~-0.45) (Fig. 11, panel c). This provides a further confirmation of the inapplicability of the method in case #3.

In general, it can be noted that ΔTEC_{SAR} maps show a finer structuring than the ΔTEC_{GNSS} ones. This is due to the finer spatial resolution reached by InSAR imaging than GNSS mapping (see Section II). The latter is based on an interpolation procedure, which produces a smoothing of ΔTEC. Then, we do not expect to fully resolve the ΔTEC_{SAR} map with the ΔTEC_{GNSS} map.

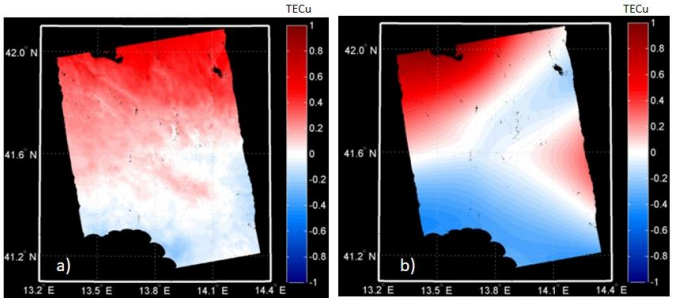

Fig. 9 Case study #1- Maps of ΔTEC_{SAR} (panel a) and ΔTEC_{GNSS} (panel b). The colorbar expresses, in TECu, the TEC variation between 1 July 2007 and 16 August 2007

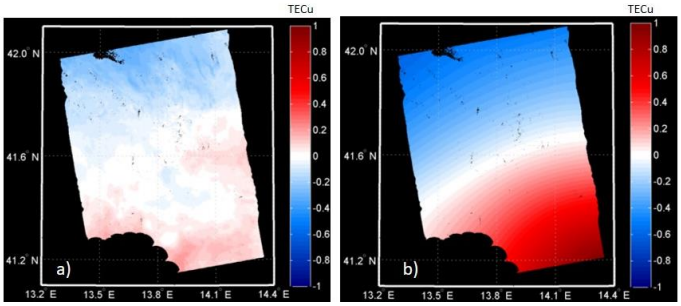

Fig. 10 Case study #2 – Maps of ΔTEC_{SAR} (panel a) and ΔTEC_{GNSS} (panel b). The colorbar expresses, in TECu, the TEC variation between 16 August 2007 and 1 October 2007

$|\Delta TEC_{SAR}|$ values are generally underestimated with respect to $|\Delta TEC_{GNSS}|$ ones. These differences may arise from several factors, among which the different geometry of the two TEC measurements, the contribution of the plasmasphere to the GNSS-TEC, the residual tropospheric effects, that play the leading roles.

In the specific, we compare slant ΔTEC_{SAR} with vertical ΔTEC_{GNSS}, the latter to minimize satellites-receivers biases (see, e.g [23]) and to obtain values TEC that are independent from the geometry of observation (i.e. not dependent on the relative position between the GNSS receivers at ground and the GPS satellites). A possible overcome of this issue, could be the use of slant ΔTEC_{GNSS} by considering a more severe elevation mask (>> 20° as here adopted). The drawback of this approach is the significant reduction of the number of IPP's, that may lead to a worsening of the interpolation procedure. On the other hands, we expect a significant contribution from free electrons in the lower parts of the plasmasphere (below approximately 3.2 Earth's *radii*, 20200 km), not crossed by SAR but by GNSS signals. Yizengaw et al. [24] estimated the relative contribution of the plasmaspheric electron content to the ground based GPS TEC by using two independent observations,

the TEC from ground based GPS network (Global Positioning System-satellite orbits is about 20200 km) and from GPS on board of JASON-1 Satellite (satellite orbit about 1300 km). This plasmaspheric contribution results to be of the order of 30% at mid-latitude during night-time. Moreover, the ALOS-PALSAR orbit (about 700 km altitude) is lower than the JASON-1 Satellite orbit, and this should further contribute to underestimate the TEC from InSAR of about a 10%, as shown by Lilensten and Bailey (2002) [25] that computed the TEC from the ionospheric bottom up to 3000 km with a step of 100 km.

Some residual tropospheric effects may also affect the correlation between the two ΔTEC measurements, following from the deviation from the ideal |R|=1 conditions in the correlation between the unwrapped phase and the integral of the azimuth shifts.

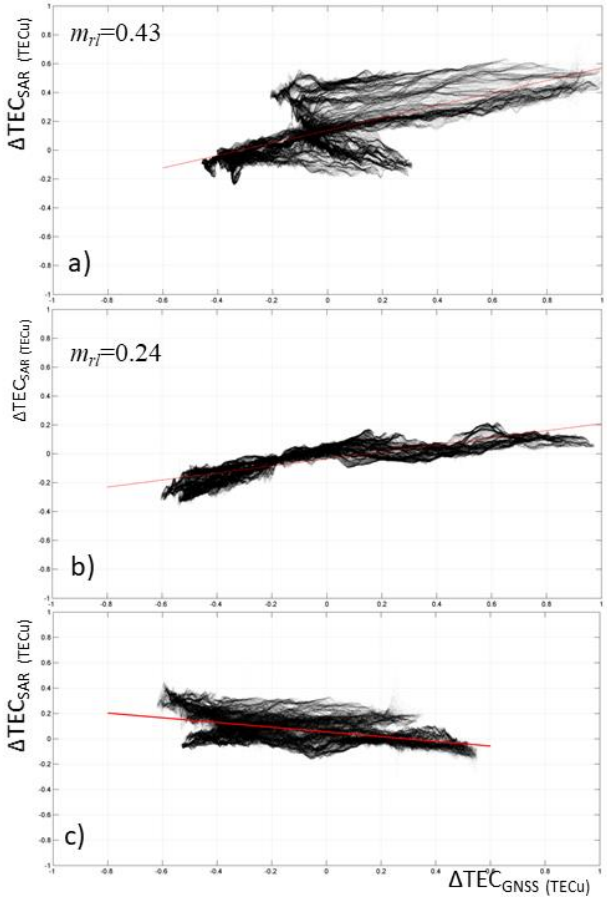

Fig. 11 Scatter plot of ΔTEC_{SAR} vs ΔTEC_{GNSS} for (a) the first case study (master: 1 July 2007 and slave: 16 August 2007); (b) the second case study (master: 16 August 2007 and slave: 1 October 2007); (c) the third case study (master: 1 July 2007 and slave: 1 October 2007. In red, the regression line is plotted. The value of the slope of the linear regression fit, m_{rl} , is reported in the plot for the first (a) and second (b) case study.

IV. Conclusions

Three night-time ALOS-PALSAR images over Italy, acquired under quiet geomagnetic conditions, are selected to investigate the effects of the ionospheric plasma, crossed by the SAR signals, on the interferometric phase. The study is supported by a dense network of GNSS receivers deployed over Italy (RING), which provides ionospheric measurements here adopted as representative of the "true ionosphere". In addition, the HF radar located in Rome (41.8 ° N, 12.5 ° E) is used to reveal sporadic formation of electron density layers, Es, around the SAR passages that may cause azimuth streaks. The effect of Es is found in two out of the three case studies here investigated.

A method, based on the correlation analysis between the integral of the azimuth shifts and the unwrapped phase, is applied in order to assume if the tropospheric contribution to the InSAR images can be negligible with respect to the ionospheric effect.

This assumption, found to be reasonable in two (out of three) cases, allows the retrieval of spatial and temporal TEC variations from InSAR, named ΔTEC_{SAR}.

To check for the reliability of the TEC variation found in such a way, ΔTEC_{SAR} is compared against the experimental, independent ΔTEC_{GNSS} obtained from the RING network. ΔTEC_{GNSS} is evaluated by assuming that the ionosphere is a thin ionized layer at 350 km above the Earth's surface and that it is "frozen" within a 5-minutes' window around the SAR passages.

In the two successful cases, ΔTEC_{SAR} and ΔTEC_{GNSS} maps are quite well correlated: R~0.67 and R~0.83. On the average, $|\Delta TEC_{SAR}|$ values are lower than $|\Delta TEC_{GNSS}|$ ones and some factors have been highlighted to be responsible for it. One factor is the plasmaspheric contribution, expected to range between 10% and 30% of the total amount of TEC. In fact, free electrons in the bottom part of the plasmasphere (below about 20200 km) are accounted in ΔTEC_{GNSS} measurements, but not in the ΔTEC_{SAR}, because of the SAR altitude. In addition, geometrical factors may affect ΔTEC_{SAR} and ΔTEC_{GNSS} comparisons. Other sources reducing the correlation have been identified in the different geometry of the observation and in residual tropospheric effects.

After a proper statistical assessment, which must also account for different seasonal, geographical, diurnal and geospace conditions, and bearing in mind the features of the proposed technique, TEC determination from SAR would significantly contribute to the monitoring and investigation of the ionospheric plasma. This would allow TEC determination with the spatial resolution given by SAR imaging (e.g., $8.33°\cdot10^{-4}$ latitude x $8.33°\cdot10^{-4}$ longitude in the considered cases), currently not reachable with ground based techniques.

Acknowledgements

The ALOS PALSAR data was provided by ESA through CAT1 proposal 26350 “Constraining Seismic Hazard Models with InSAR and GPS (CHARMING)”.

The ionograms are provided by www.eswua.ingv.it/.

V. References

[1] X. Zhou, N.-B. Chang and S. Li, "Applications of SAR interferometry in earth and environmental science research," *Sensors*, vol. 9, no. 3, pp. 1876-1912, 2009.

[2] F. J. Meyer and J. Nicoll, "The impact of the ionosphere on interferometric SAR processing," *Geoscience and Remote Sensing Symposium, 2008. IGARSS 2008. IEEE International*, vol. 2, pp. II-391 - II-394, 2008.

[3] M. Jehle, O. Frey, D. Small and E. Meier, "Measurement of Ionospheric TEC in Spaceborne SAR Data," *IEEE Transactions on Geoscience and Remote Sensing*, vol. 48, no. 6, pp. 2460-2468, 2010.

[4] F. Meyer, R. Bamler, N. Jakowski and T. Fritz, "The potential of low-frequency SAR systems for mapping ionospheric TEC distributions," *IEEE Geoscience and Remote Sensing Letters*, vol. 3, no. 4, pp. 560-564, 2006.

[5] A. L. Gray, K. E. Mattar and G. Sofko, "Influence of ionospheric electron density fluctuations on satellite radar interferometry," *Geophysical Research Letters*, vol. 27, no. 10, pp. 1451-1454, 2000.

[6] K. E. Mattar and A. L. Gray, "Reducing ionospheric electron density errors in satellite radar interferometry applications," *Canadian Journal of Remote Sensing*, vol. 28, no. 4, pp. 593-600, 2002.

[7] F. J. Meyer and P. S. Agram, "Developing an Error Model for Ionospheric Phase Distortions in L-Band SAR and InSAR Data," in *FRINGE’15: Advances in the Science and Applications of SAR Interferometry and Sentinel-1 InSAR Workshop*, Frascati, 23-27 March 2015.

[8] F. J. Meyer, "Performance requirements for ionospheric correction of low-frequency SAR data," *IEEE Transactions on Geoscience and Remote Sensing*, vol. 49(10), pp. 3694-3702, 2011.

[9] A. C. Chen and H. A. Zebker, "Reducing ionospheric effects in InSAR data using accurate coregistration," *EEE Transactions on Geoscience and Remote Sensing*, vol. 52, no. 1, pp. 60-70, 2014.

[10] R. Scheiber and A. Moreira, "Coregistration of interferometric SAR images using spectral diversity," *IEEE Transactions on Geoscience and Remote Sensing*, vol. 38, no. 5, pp. 2179-2191, 2000.

[11] N. B. D. Bechor and H. A. Zebker, "Measuring two-dimensional movements using a single InSAR pair," *Geophysical research letters*, vol. 33, no. 16, p. L16311, 2006.

[12] C. Cesaroni, L. Spogli, L. Alfonsi, G. De Franceschi, L. Ciraolo, J. Francisco, G. Monico, C. Scotto, V. Romano, M. Aquino and B. Bougard, "L-band scintillations and calibrated total electron content gradients over Brazil during the last solar maximum," *Journal of Space Weather and Space Climate*, vol. 5, no. A36, 2015.

[13] A. J. Mannucci, B. D. Wilson and D. N. Yuan, "A global mapping technique for GPS-derived ionospheric total electron content measurement," *Radio science*, vol. 33, no. 3, pp. 565-582, 1998.

[14] R. Sibson, "A brief description of natural neighbor interpolation (Chapter 2)," in *V. Barnett. Interpreting Multivariate Data*, Chichester: John Wiley, 1981, pp. 21-36.

[15] C. Cesaroni, "A multi instrumental approach to the study of equatorial ionosphere over South-America," PhD dissertation, DIFA, Bologna, Italy, 2015b.

[16] L. Perrone and G. De Franceschi, "Solar, ionospheric and geomagnetic indices," *Annals of Geophysics*, vol. 41, no. 5-6, p. 843–855, 1998.

[17] C. Bianchi, J. A. Baskaradas, M. Pezzopane, U. Sciacca and E. Zuccheretti, "Fading in the HF ionospheric channel and the role of irregularities," *Advances in Space Research* , vol. 52, no. 3, p. 403–411, 2013.

[18] W. R. Piggott and K. Rawer, "U. R. S. I. handbook of ionogram interpretation and reduction," World Data Centre for Solar-Terrestrial Physics, NOAA, Boulder, Colorado, 1972.

[19] J. D. Whitehead, "Recent work on mid-latitude and equatorial sporadic-E," *Journal of Atmospheric and Terrestrial Physics*, vol. 51, no. 5, pp. 401-424, 1989.

[20] G. Didebulidze , G. Dalakishvili, L. Lomidze and G. Matiashvili, "Formation of sporadic-E (Es) layers under the influence of AGWs evolving in a horizontal shear flow," *Journal of Atmospheric and Solar-Terrestrial Physics*, vol. 136, p. 163–173, 2015.

[21] R. D. Hunsucker, "Atmospheric gravity waves generated in the high-latitude ionosphere: A review," *Reviews of Geophysics*, vol. 20, no. 2, pp. 293-315, 1982.

[22] J. Maeda, T. Suzuki, M. Furuya and K. Heki, "Imaging the midlatitude sporadic E plasma patches," *Geophysical Research Letters*, vol. 43, p. 1419–1425, 2016.

[23] L. Ciraolo, F. Azpilicueta, C. Brunini, A. Meza and S. Radicella, "Calibration errors on experimental slant total electron content (TEC) determined with GPS," *Journal of Geodesy*, vol. 81, no. 2, pp. 111-120, 2007.

[24] E. Yizengaw, M. Moldwin, D. Galvan , B. Iijima, A. Komjathy and A. J. Mannucci, "Global plasmaspheric TEC and its relative contribution to GPS TEC," *Journal of Atmospheric and Solar-Terrestrial Physics*, vol. 70, no. 11, pp. 1541-1548., 2008.

[25] J. Lilensten and P. Blelly, "The TEC and F2 parameters as tracers of the ionosphere and thermosphere," *Journal of atmospheric and solar-terrestrial physics*, vol. 64, no. 7, pp. 775-793, 2002.